mathematics

MDPI

Article

Analysis of Non-Linear Radiation and Activation Energy Analysis on Hydromagnetic Reiner–Philippoff Fluid Flow with Cattaneo–Christov Double Diffusions

Mohamed E. Nasr [1], Machireddy Gnaneswara Reddy [2], W. Abbas [3], Ahmed M. Megahed [4,*], Essam Awwad [1,4] and Khalil M. Khalil [1,4]

[1] Department of Mathematics, College of Science and Arts—Gurayat, Jouf University, Sakakah 77454, Saudi Arabia; menasr@ju.edu.sa (M.E.N.); emawwad@ju.edu.sa (E.A.); kmshalaby@ju.edu.sa (K.M.K.)
[2] Department of Mathematics, Acharya Nagarjuna University Campus, Ongole 523 001, India; gnaneswarareddym@anu.ac.in (M.G.R.)
[3] Basic and Applied Science Department, College of Engineering and Technology, Arab Academy for Science, Technology and Maritime Transport, Cairo 11511, Egypt; wael_abass@aast.edu (W.A.)
[4] Department of Mathematics, Faculty of Science, Benha University, Benha 13518, Egypt
* Correspondence: ahmed.abdelbaqk@fsc.bu.edu.eg

Abstract: Using magnetohydrodynamics (MHD), the thermal energy and mass transport boundary layer flow parameters of Reiner–Philippoff fluid (non-Newtonian) are numerically investigated. In terms of energy and mass transfer, non-linear radiation, Cattaneo–Christov double diffusions, convective conditions at the surface, and the species reaction pertaining to activation energy are all addressed. The stated governing system of partial differential equations (PDEs) is drained into a non-linear differential system using appropriate similarity variables. Numerical solutions are found for the flow equations that have been determined. Two-dimensional charts are employed to demonstrate the flow field, temperature and species distributions, and rate of heat and mass transfers for the concerned parameters for both Newtonian and Reiner–Philippoff fluid examples. The stream line phenomenon is also mentioned in this paper. A table has also been utilized to illustrate the comparison with published results, which shows that the current numerical data are in good accord. The findings point to a new role for heat and mass transfer. According to the findings, increasing values of solutal and thermal relaxation time parameters diminish the associated mass and thermal energy layers. The current study has significant ramifications for chemical engineering systems.

Keywords: Cattaneo–Christov double diffusions; non-linear radiation; activation energy; convective conditions; Reiner–Philippoff fluid

MSC: 76Wxx; 76A05; 65L10

Citation: Nasr, M.E.; Gnaneswara Reddy, M.; Abass, W.; Megahed, A.M.; Awwad, E.; Khalil, K.M. Analysis of Non-Linear Radiation and Activation Energy Analysis on Hydromagnetic Reiner–Philippoff Fluid Flow with Cattaneo–Christov Double Diffusions. *Mathematics* **2022**, *10*, 1534. https://doi.org/10.3390/math10091534

Academic Editor: Francisco Chiclana

Received: 6 April 2022
Accepted: 29 April 2022
Published: 3 May 2022

1. Introduction

Because of their numerous uses in industrial fields such as cooling systems, paint, adhesives, food processing, drilling rigs, nuclear reactors, organic materials, molten polymers, and inks, the study of non-Newtonian fluids has received a lot of attention. The Navier–Stokes theory cannot be used to explain these types of liquids. In these types of fluids, the order of the differential systems is frequently higher. There are various models of non-Newtonian liquids, which are commonly divided into three categories: differential, rate, and integral types. One of the non-Newtonian models, Reiner–Philippoff fluid, is considered in this work. Some investigations related to the Reiner–Philippoff model are described in depth; for example, see [1–5]. The heat transmission phenomenon is the most essential aspect in industrial and manufacturing systems. The fundamental explanation

for the occurrence of such a phenomenon is temperature variations between or within a medium. Fourier's law of heat conduction has been used to analyze heat transfer difficulties during the past two decades. This law's fundamental difficulty is that it provides a parabolic energy equation in which any initial disturbance is detected throughout the entire system. Cattaneo modified Fourier's law of heat conduction to account for this complexity by include the thermal relaxation period. As a result, several researchers [6–11] reported on the study of Cattaneo and Christov (CC) of heat and mass flux on various non-Newtonian fluids.

Several researchers have accomplished various types of study involving the magnetohydrodynamics (MHD) flow of non-Newtonian fluids because of its significant applicability in manufacturing and scientific domains such as plasma confinement and liquid metal fabrication. Many studies on the magnetohydrodynamic laminar flow of non-Newtonian liquids across various surfaces have been published [12–22]. The spontaneous exudation of energy from any materials having a higher temperature than absolute zero is called thermal radiation. It has extensive applications in manufacturing industries such as nuclear power plants, missiles, gas turbines, energy transfer furnaces, satellites, and space vehicles. Many researchers are investigating the flow problems by taking account of the non-linear thermal radiation effect. The influence of viscous dissipation and non-linear thermal radiation on the Casson fluid stream past a moving sheet was inspected by Kumar et al. [23]. Qayyum et al. [24] demonstrated the consequence of radiation effect on the MHD flow of nanoliquid through a stretching cylinder. The influence of thermal radiation on the stream of Sisko nanoliquid past an elastic sheet with chemical reaction was explored by Prasannakumara et al. [25]. Hayat et al. [26] described the effect of non-linear thermal radiation on the stream of Jeffrey nanoliquid over an extended surface. Khan et al. [27] explored the Williamson liquid flow past a surface on taking non-linear thermal radiation into account.

The activation energy is demarcated as the least amount of energy that reactants should acquire before involving in a chemical reaction. The chemical reaction along with activation energy has important applications in food processing, chemical engineering, geothermal reservoirs, and oil emulsions. Khan et al. [28] analyzed the impact of activation energy and thermal radiation on the flow of magnetized Casson nanoliquid past a sheet. The flow pattern of Prandtl–Eyring nanoliquid generated by a spinning disk with the impact of ohmic heating and the activation energy was scrutinized emphatically by Qayyum et al. [29]. The consequence of ohmic heating with activation energy on the nanofluid flow over a rotating disk was reported by Kotresh et al. [30]. Khan and Alzahrani [31] explained the aspects of activation energy with non-linear thermal radiation on the MHD flow of Walter-B nanoliquid. Jayadeva murthy et al. [32] scrutinized the hybrid nanoliquid stream through a revolving disk with bio-convection effect and activation energy. Recently, numerous researchers examined the behaviour of liquid in the presence of convective boundary constraints when taking account of several influencing factors. Shehzad et al. [33] inspected the effect of convective heat and mass conditions on nanofluid flow over an expanding surface. The nanofluid flow over a disk with convective conditions was elucidated by Prasannakumara et al. [34]. Hayat et al. [35] investigated the aspects of convective conditions in the fluid stream over a curved surface. Gireesha et al. [36] discussed the effect of non-linear thermal radiation with convective conditions on the Oldroyd-B nanoliquid flow past an elastic surface. Muhammad et al. [37] presented a report on the stream of Jeffrey liquid suspended with nanoparticles with convective conditions. The current study's scientific innovation may be seen in the examination of CC double diffusions (CCDD) flow on hydromagnetic activation energy in the flow of Reiner–Philippoff fluid.

2. Mathematical Modeling

In two dimensions (2D) and incompressible case, the flow of a non-Newtonian Reiner–Philippoff liquid across a moving stretching surface was investigated. Figure 1 shows a flow diagram of physical geometry. We can choose x-axis along the surface, and y-axis is assumed to be normal to the surface plane. The fluid is drawn via a slit in the sheet where the origin is located. In this study, a uniform magnetic field is considering normal to the sheet with strength B. Furthermore, the absence of Hall current is associated with the existence of magnetic field, which may impact fluid flow motion. It is assumed that the non-Newtonian fluid is transported along the surface with stretching nonlinear velocity $u_w(x) = ax^{1/3}$ in x-axis direction. The variables are the non-Newtonian fluid concentration C_w and the non-Newtonian fluid temperature T_w at the stretching surface, respectively. The ambient thermal and species values are T_∞ and C_∞. Using generalized Fick's and Fourier relations, Cattaneo–Christov double diffusions (CCDD) are utilized to achieve energy and species transport. The applied magnetic field is being used in the vertical direction of fluid flow. The thermal equation takes into account non-linear radiation, and the activation energy is taken into account in the species equation. In this model, the convective energy and species conditions are also assimilated at the boundary.

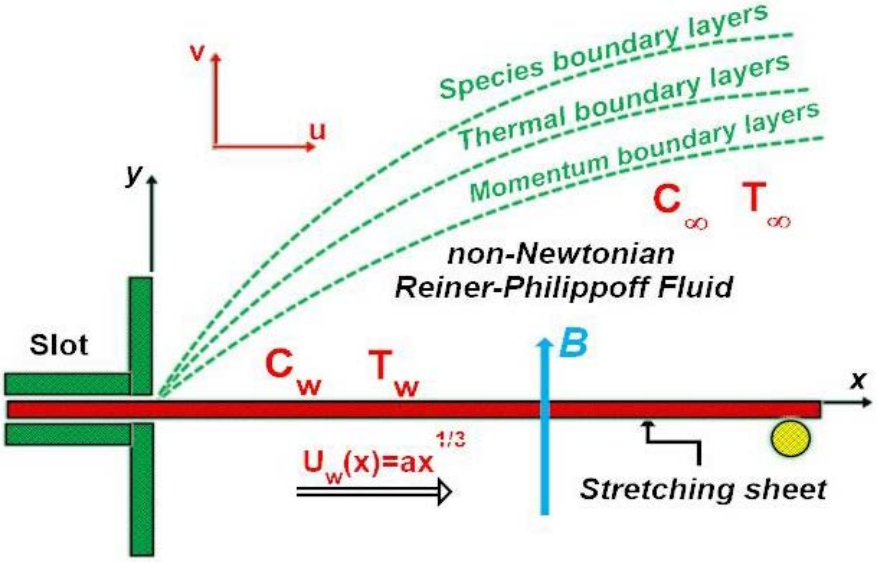

Figure 1. Geometry Flow Modeling.

The non-Newtonian Reiner–Philippoff fluid, the description relations between shear-strain $\frac{\partial u}{\partial y}$ and shear-stress τ are defined as [2–4]

$$\frac{\partial u}{\partial y} = \frac{\tau}{\mu_\infty + \frac{(\mu_0 - \mu_\infty)}{1 + \left(\frac{\tau}{\tau_S}\right)^2}} \tag{1}$$

Here, τ_S is the reference shear-stress and τ is the shear-stress, μ_∞ is the upper limiting viscosity, and μ_0 is the zero shear viscosity.

It is clear that the Equation (1) represents the flow function and the non-dimensional flow function is given by

$$f(\xi) = \frac{\xi}{1 + \frac{(\lambda - 1)}{1 + \xi^2}} \tag{2}$$

in which $\lambda = \frac{\mu_0}{\mu_\infty}$, and $\xi = \frac{\tau}{\tau_S}$.

It is of note that the fluid behaves for the Newtonian flow case if $\lambda = 1$ and Reiner–Philippoff flow case (non-Newtonian) if $\lambda \neq 1$.

Aforementioned assumptions and boundary layer approximations are employed, then the equations of total mass, fluid flow along thermal and species are written as [6,7,15,26]

$$\frac{\partial u}{\partial x} + \frac{\partial u}{\partial y} = 0, \tag{3}$$

$$u\frac{\partial u}{\partial x} + v\frac{\partial u}{\partial y} = \frac{1}{\rho}\frac{\partial \tau}{\partial y} - \frac{\sigma B^2(x)}{\rho}u, \tag{4}$$

$$u\frac{\partial T}{\partial x} + v\frac{\partial T}{\partial y} + \lambda_t \left(\begin{array}{c} u^2\frac{\partial^2 T}{\partial x^2} + v^2\frac{\partial^2 T}{\partial y^2} + 2uv\frac{\partial^2 T}{\partial x \partial y} + \\ \left(u\frac{\partial u}{\partial x} + v\frac{\partial u}{\partial y}\right)\frac{\partial T}{\partial x} + \left(u\frac{\partial u}{\partial x} + v\frac{\partial u}{\partial y}\right)\frac{\partial T}{\partial y} \end{array} \right) = \alpha\frac{\partial^2 T}{\partial y^2} - \frac{1}{\rho c_p}\frac{\partial q_r}{\partial y} + \frac{\sigma B^2}{\rho c_p}u^2 \tag{5}$$

$$u\frac{\partial C}{\partial x} + v\frac{\partial C}{\partial y} + \lambda_c \left(\begin{array}{c} u^2\frac{\partial^2 C}{\partial x^2} + v^2\frac{\partial^2 C}{\partial y^2} + 2uv\frac{\partial^2 C}{\partial x \partial y} + \\ \left(u\frac{\partial u}{\partial x} + v\frac{\partial u}{\partial y}\right)\frac{\partial C}{\partial x} + \left(u\frac{\partial u}{\partial x} + v\frac{\partial u}{\partial y}\right)\frac{\partial C}{\partial y} \end{array} \right) = D\frac{\partial^2 C}{\partial y^2} - k_r(C - C_\infty)\left(\frac{T}{T_\infty}\right)^m \exp\left[\frac{-E_a}{\kappa T}\right] \tag{6}$$

The problem of approximate boundary constraints at the surface of a flowing sheet and liquid at infinity are [3,7,34]

$$u = u_w(x) = ax^{1/3}, \;\; v = 0, \;\; -k\frac{\partial T}{\partial y} = h_1(T_w - T), \;\; -D\frac{\partial C}{\partial y} = h_2(C_w - C) \quad \text{at } y = 0,$$

$$u \to 0, \; T \to T_\infty, \;\; C \to C_\infty \;\text{ as }\; y \to \infty. \tag{7}$$

The first part of Equation (7) physically signifies that the stretched sheet's relationship is non-linear, which has an impact on fluid flow and heat transmission mechanisms. The Rosseland radiative energy flux [13,24], which is utilized in Equation (5), is manifested by

$$q_r = -\frac{4\sigma^*}{3k^*}\frac{\partial T^4}{\partial y} = -\frac{16\sigma^* T_\infty^3}{3k^* k_\infty} \tag{8}$$

Here σ^* and k^* symbols indicate the Stefan–Boltzmann constant and mean absorption coefficient accordingly.

Define the following similarity and dimensionless variables:

$$\zeta = \sqrt{\frac{a}{\nu}}\frac{y}{x^{1/3}}, \psi = \sqrt{a\nu}x^{2/3}, \tau = \rho\sqrt{a^3\nu}g(\eta), \; \theta(\eta) = \frac{T - T_w}{T_w - T_\infty}, \; \phi(\eta) = \frac{C - C_w}{C_w - C_\infty}, \; \gamma = \frac{\tau_S}{\rho\sqrt{a^3\nu}},$$

$$\gamma = \frac{\tau_S}{\rho\sqrt{a^3\nu}}, M = \frac{\sigma B_0^2}{\rho a}, \Pr = \frac{\nu}{\alpha}, \Gamma_t = \lambda_1 u_w, Rd = \frac{16\sigma^* T_\infty^3}{3k^* k_\infty}, \theta_w = \frac{T_w}{T_\infty}, Ec = \frac{u_w^2}{(T_w - T_\infty)c_p},$$

$$Br = \Pr Ec, \sigma_r = \frac{k_r^2}{a}, \delta = \frac{T_w - T_\infty}{T_\infty}, E = \frac{E_a}{\kappa T_\infty}, \Gamma_c = \lambda_2 u_w, Sc = \frac{\nu}{D}, Bi_1 = \frac{h_1 u_w}{k_1 a}\sqrt{\frac{\nu}{a}}, Bi_2 = \frac{h_2 u_w}{Da}\sqrt{\frac{\nu}{a}} \quad (9)$$

It is clear and obvious that the conservation of total mass Equation (3) is satisfied. Utilizing Equation (8) in the above modelling system of partial differential Equations (PDE's) (4)–(6), we obtain the following system of non-linear ODE's.

$$g = f''\frac{g^2 + \lambda\gamma^2}{g^2 + \gamma^2}, \quad (10)$$

$$g' = -\frac{2}{3}ff'' + \frac{1}{3}f'^2 + Mf', \quad (11)$$

$$\left(1 + (\frac{4}{3}Rd(1 + (\theta_w - 1)\theta)^3)\theta'\right)' + \frac{2}{3}\Pr f\theta' + \Pr\Gamma_t(ff'\theta' + \eta f^2\theta'') + MBrf''^2 = 0, \quad (12)$$

$$\phi'' + \frac{2}{3}Scf\phi' + Sc\Gamma_c(ff'\phi' + \eta f^2\phi'') - Sc\sigma_r(1 + \delta\theta)^m \phi\exp\left(-\frac{E}{1 + \delta\theta}\right) = 0, \quad (13)$$

and the simplified dimensionless boundary conditions are

$$f(0) = 0,\ f'(0) = 1,\ \theta'(0) = -Bi_1(1 - \theta(0)),\ \phi'(0) = -Bi_2(1 - \phi(0)),$$

$$f'(\infty) \to 0,\ \theta(\infty) \to 0,\ \phi(\infty) \to 0 \quad (14)$$

in which ς is the dimensionless similarity variable, M is the magnetic field parameter, λ is the Reiner–Philippoff fluid parameter, Rd is the radiation parameter, θ_w is the temperature ratio parameter, Γ_t is the thermal relaxation time parameter, Br is the Brinkman parameter, Sc is the Schmidt number, σ_r is the local chemical reaction parameter, the dimensionless activation energy variable is denoted by E, the solutal relaxation time parameter is denoted by Γ_c, Bi_1, Bi_2 are thermal and concentration Biot numbers, and θ, ϕ are correspondingly, the non-dimensional thermal and mass functions.

Engineering Physical Quantities

The local Nusselt number Nu_x is given by

$$Nu_x = \frac{xq_w}{k(T_w - T_\infty)}, \quad (15)$$

Here the expression q_w indicates the heat flux defined by

$$q_w = -k\left(\frac{\partial T}{\partial y}\right)_{y=0} + q_r. \quad (16)$$

The local Sherwood number Sh_x is represented by

$$Sh_x = \frac{xq_m}{D(C_w - C_\infty)}, \tag{17}$$

in which the expression q_m indicates the species flux and is represented by

$$q_m = -D\frac{\partial C}{\partial y}, \tag{18}$$

The dimensionless heat and mass transfer rates are calculated by employing the Equation (8)

$$Nu_x \,\mathrm{Re}_x^{-1/2} = -(1+\frac{4}{3}Rd((\theta_w - 1)\theta(0)+1)^3)\theta'(0), \tag{19}$$

and

$$Sh_x \,\mathrm{Re}_x^{-1/2} = -\phi'(0). \tag{20}$$

3. Numerical Scheme

A numerical method with the use of boundary conditions as indicated in Equation (14), Runge-Kutta of order four, is utilized in Mathematica to solve a non-linear system of ODEs (see Equations (10)–(13)). The equations that result are higher-order ODEs. To begin, we reduce these higher-order ODEs to first-order form as follows

$$f = Y_1, \;\; f' = Y_2 \tag{21}$$

$$g = Y_3, \;\; g' = Y_4 \tag{22}$$

$$Y_2' = Y_3\frac{Y_3^{\,2} + \gamma^2}{Y_3^{\,2} + \lambda\gamma^2} \tag{23}$$

$$Y_4 = \frac{-2}{3}Y_1Y_2' + \frac{1}{3}Y_2^{\,2} + MY_2 \tag{24}$$

$$\theta = Y_5, \;\; \theta' = Y_6 \tag{25}$$

$$Y_6' = \frac{1}{\eta Y_1^{\,2}}\left(-\Pr\Gamma_2 Y_1Y_2Y_6 - MBrY_2^{\,2} - \frac{2}{3}\Pr Y_1Y_6 - \left[1+(\frac{4}{3}Rd(1+(\theta_w-1)Y_5)^3)Y_6\right]\right) \tag{26}$$

$$\phi = Y_7, \;\; \phi' = Y_8 \tag{27}$$

$$Y_8' = \frac{1}{1+Sc\Gamma_c\eta Y_1^{\,2}}\left(-\frac{2}{3}ScY_1Y_8 - Sc\Gamma_c Y_1Y_2Y_8 + Sc\sigma_r(1+\delta Y_5)Y_7\exp(\frac{-E}{1+\delta Y_5})\right) \tag{28}$$

The following are the transformed boundary conditions

$$Y_1(0) = 0, \; Y_2(0) = 1, \;\; Y_6(0) = -Bi_1(1-Y_5(0)), \; Y_8(0) = -Bi_2(1-Y_7(0)), \tag{29}$$

$$Y'_2(0) = \varepsilon_1, \;\; Y_5(0) = \varepsilon_2, \; Y_7(0) = \varepsilon_3, \tag{30}$$

Iterations of the shooting method are used to guess $\varepsilon_1, \varepsilon_2,$ and ε_3 until the outer boundary requirements (14) are met. The resulting differential equations can be integrated

using the fourth-order Runge-Kutta integration scheme once convergence is reached. The method is repeated until the results are as accurate as we want them to be 10^{-6}.

4. Graphical Discussion

The final governing modeled flow Equations (10)–(14) are highly non-linear and coupled. Therefore, we did not find the exact solution expressions for the modeled problem. Hence, we can find the numerical solution of the Equations (10)–(14) along boundary constraints (15) through the Runge-Kutta fourth-order scheme along with a shooting procedure. It is worth mentioning that the present study is a generalization of the previously published work of Ganesh Kumar et al. [3]. Here, in the flow of Reiner–Philippoff fluid with non-linear radiation and convective conditions at the surface, we investigate the effect of Cattaneo–Christov double diffusions flow on hydromagnetic activation energy. The major goal of the current physical problem is to control the heat and mass transfer mechanisms due to their important applications in various fields, such as electronic device cooling, steam-electric power generation, and in characterizing and diagnosing diseases. This goal can be achieved by selecting appropriate values for the problem's governing parameters ($M, \gamma, Rd, \Gamma_t, \Gamma_c, Ec, \theta_w, Sc, E, \sigma_r, \delta, Bi_1$ and Bi_2). Some of these parameters, such as the Prandtl number $\Pr$, can be selected based on the fluid type. Thus, following Ganesh Kumar et al. [3], the following constants have been adopted: $M = 0.5$, $\gamma = 0.5$, $Rd = 2.0$, $\theta_w = 0.1$, $\Pr = 3.5$, $\Gamma_t = \Gamma_c = 0.2, Ec = 0.5, Sc = 2.0, E = 0.2, \sigma_r = \delta = 0.1$, $Bi_1 = Bi_2 = 0.2$, for Newtonian fluid flow case when $\lambda = 1.0$ and Reiner–Philippoff fluid case when $\lambda \neq 1.0$.

Table 1 displays the validation of the present results with the outcomes of the available literature of Reddy et al. [3] and Sajid et al. [4]. The numerical values are of the rate of heat transfer for the Prandtl number $\Pr$ for $\lambda = 1$, $Rd = \Gamma_t = \Gamma_c = Ec = \sigma_r = 0$. From this table, it is observed that the accuracy of the current numerical procedure and the outcomes of the existing results are in good agreement from the analysis.

Table 1. Comparison values of Nusselt number for distinct values of $\Pr$.

Pr	Reddy et al. [3]	Sajid et al. [4]	Present Values
1.0	0.556060	0.556065	0.556067
1.5	0.727935	0.727928	0.727934
2.0	0.873989	0.873992	0.873990
2.5	1.012062	1.012056	1.012061

The present analysis is carried out on the boundary layer flow of Reiner–Philippoff fluid by taking account of Cattaneo–Christov Double diffusions (CCDD) and activation energy. By selecting appropriate similarity variables, the modelled equation for the expected flow is translated to ODEs. A numerical scheme is used to provide a clear knowledge of the behaviour of flow profiles, which are strategized and deliberated with the help of graphs. The primary goal of this section is to discuss the characteristics of significant parameters such as the magnetic field parameter, temperature ratio parameter, radiation parameter, thermal relaxation time parameter, Brinkman parameter, dimensionless activation energy, local chemical reaction parameter, solutal relaxation time parameter, and thermal and concentration Biot numbers. Furthermore, numerical solutions for velocity, temperature, and concentration gradients are derived for a variety of values of relevant parameters. Additionally, the impact of several dimensionless parameters on the Nusselt number and Sherwood number are discussed by using graphs.

The influence of the magnetic parameter on velocity gradient is depicted in Figure 2. One can notice from the plotted figure that an upsurge in M declines the velocity gradient. Larger values of the magnetic parameter produce Lorentz force, which creates

resistance to fluid motion and causes declination of the fluid motion's velocity. Furthermore, the rate of declination is faster in Newtonian fluid when compared to Reiner–Philippoff liquid. Figure 3 portrays the effect of M on the thermal profile. As can be observed from the graph, increasing M increases the thermal gradient. Here, escalating values of M produces resistance to the fluid motion and improves the fluids' viscosity, which results in an inclination of thermal gradient. Furthermore, both fluids show almost the same behaviour in heat transfer for an upsurge in values of M. The actions of concentration gradient for escalating values of M are portrayed in Figure 4. The displayed graph shows that increasing the value of M improves the mass distribution. Furthermore, the rate of inclination is faster in Newtonian liquid when compared to non-Newtonian fluid. The sway of the Rdon thermal gradient is displayed in Figure 5. The upsurge in Rd improves the thermal profile. Here, inclined values of Rd produce inner heat, which obviously improves the thermal gradient. The influence of θ_w on thermal gradient is illustrated in Figure 6. One can notice from the plotted graph that the rise in values θ_w upsurges the thermal gradient. Furthermore, the rate of inclination in the thermal gradient is slightly faster in Newtonian liquid when compared to non-Newtonian liquid.

The sway of Γ_t on the thermal gradient is portrayed in Figure 7. It is detected from the plotted figure that the upsurge in the thermal relaxation time parameter escalates the thermal gradient. Furthermore, the rate of inclination is slower in Newtonian liquid when compared to Reiner–Philippoff liquid. The variation in thermal profile for diverse values of Brinkman parameter is displayed in Figure 8. Here, escalating values of Br improve the thermal gradient. Furthermore, the rate of inclination in the thermal gradient is a little bit faster in Reiner–Philippoff liquid when compared to another one. The levering of Bi_1on the thermal gradient is demonstrated in Figure 9. The heightening of the thermal Biot number heightens the thermal profile. Furthermore, both fluids show almost the same behaviour in heat transfer for an upsurge in the thermal Biot number. The pictorial representation of the behaviour of the concentration gradient for inclined values of σ_r is depicted in Figure 10. It is noted from the plotted graph that the rise in values of the local chemical reaction rate parameter declines the mass transfer. Furthermore, the initial rate of declination in the concentration gradient is faster in Reiner–Philippoff liquid when compared to another one. However, both fluids show the same mass transfer when they are near to the wall. The variation in concentration gradient for diverse values of the dimensionless activation energy parameter is illustrated in Figure 11. Here, the increase in values of E, upsurges the mass distribution. Furthermore, the rate of inclination in the concentration gradient is faster in Newtonian liquid when compared to Reiner–Philippoff liquid. The effect of Γ_c on the concentration gradient is displayed in Figure 12. Here, boost up values of the solutal relaxation time parameter boosts up the mass transfer. Furthermore, the rate of inclination in the concentration gradient is slower in Reiner–Philippoff liquid when compared to Newtonian liquid.

The sway of the radiation parameter at the heat transfer rate versus Γ_t is illustrated in Figure 13. We can observe from this graph that the rise in values of the radiation parameter decreases the heat transfer rate and the rate of declination is in Newtonian liquid when compared to Reiner–Philippoff liquid. Furthermore, the Nusselt number is a decreasing function of both the thermal relaxation time parameter and radiation parameter. The variation in the Nusselt number versus Pr for diverse values of the thermal Biot number is demonstrated in Figure 14. It is noticed from the plotted figure that an upsurge in the thermal Biot number improves the rate of heat transfer in both fluid streams and the rate of inclination in the Nusselt number is faster in Newtonian liquid when compared to Reiner–Philippoff liquid when fluids are near to the wall and shows almost the same behaviour when they are away from the boundary. Here, the Nusselt number acts as an increasing function of the Prandtl number and thermal Biot number. The variation in rate of the mass transfer versus solutal relaxation time parameter for diverse values of Sc is illustrated in Figure 15. Here, boost up values of Sc improves the mass transfer rate in both fluids. Furthermore, the Sherwood number acts as an increasing function of solutal

relaxation time parameter. Figures 16–19 portray the streamlines for diverse values of M and λ. It is manifest from these plots that the number of stream line fluid flow patterns are reduced for the higher applied magnetic field. Furthermore, it is worthy of note that the impact of the non-Newtonian liquid is greatly contrasted to the Newtonian fluid ($\lambda = 1.0$).

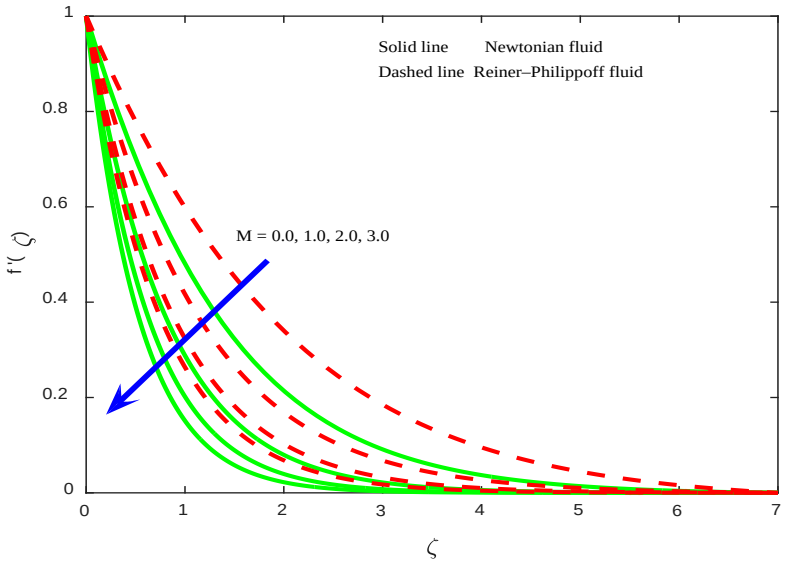

Figure 2. Velocity field for assorted values of M .

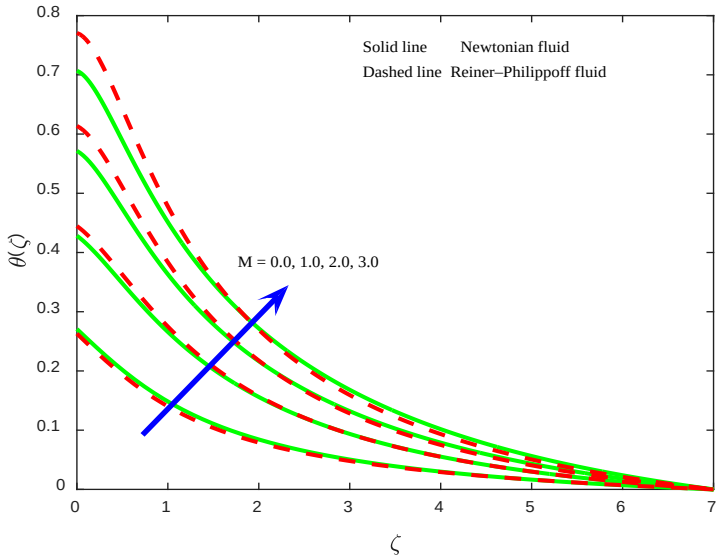

Figure 3. Temperature field for different values of M .

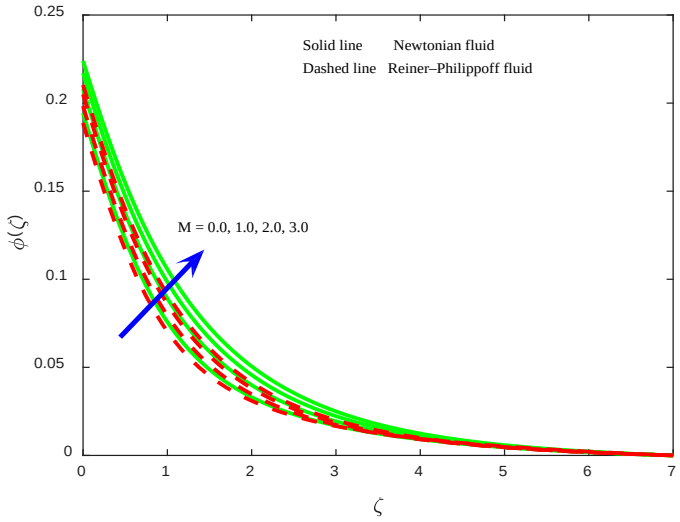

Figure 4. Concentration field for assorted values of M .

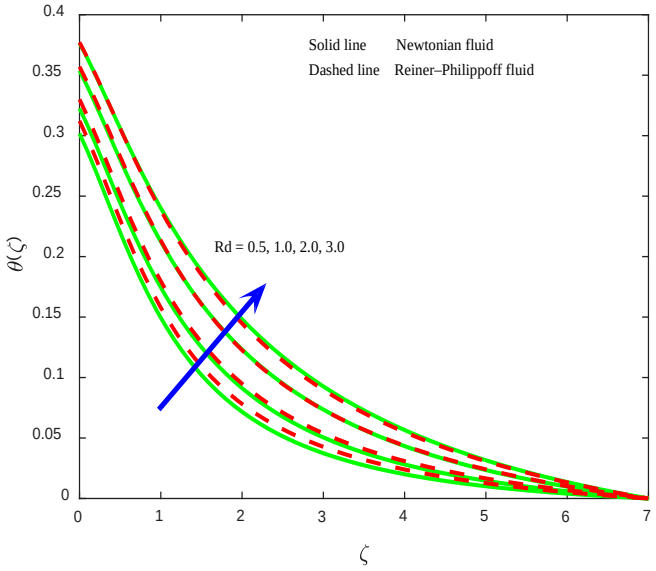

Figure 5. Temperature field for assorted values of Rd .

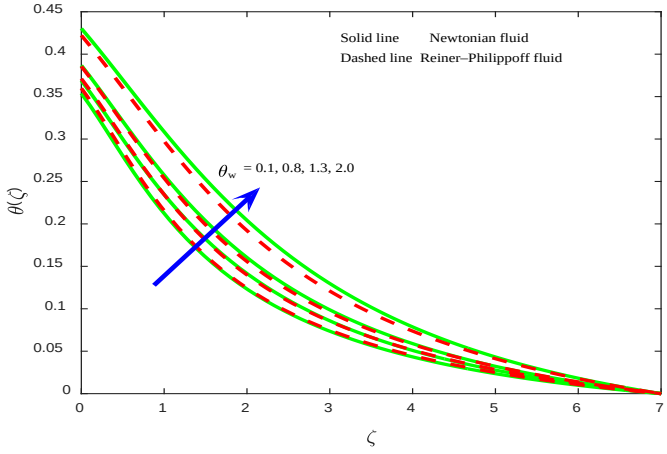

Figure 6. Temperature field for assorted values of θ_w .

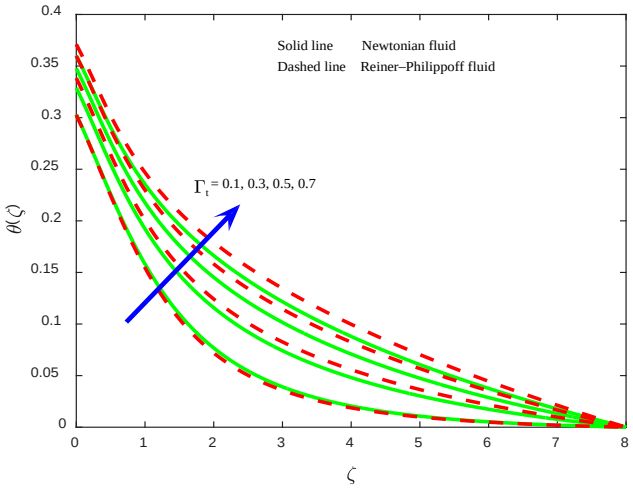

Figure 7. Temperature field for assorted values of Γ_t.

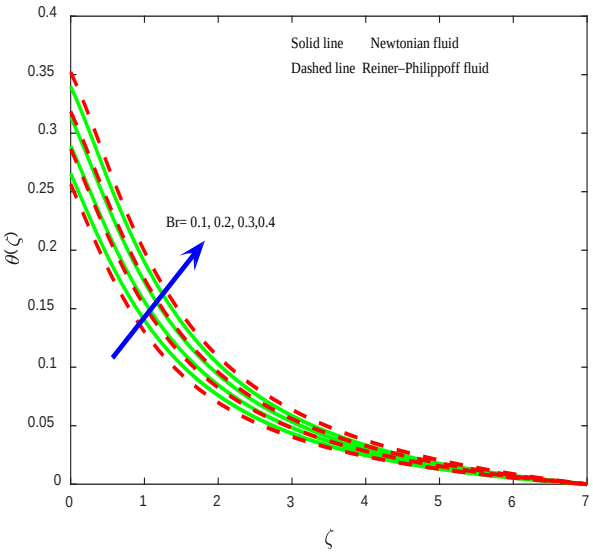

Figure 8. Temperature field for assorted values of Br.

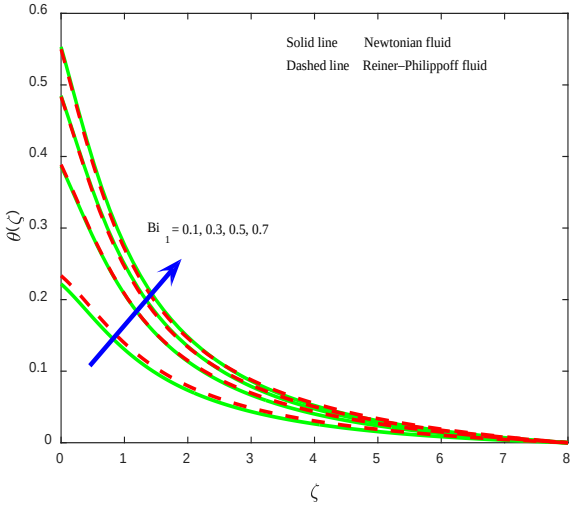

Figure 9. Temperature field for assorted values of Bi_1.

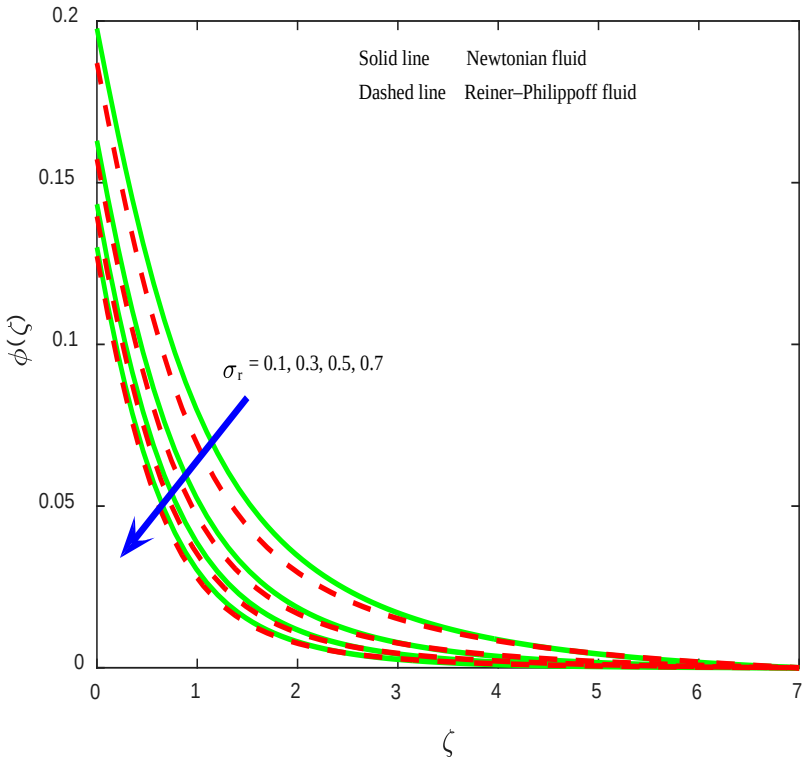

Figure 10. Concentration field for assorted values of σ_r .

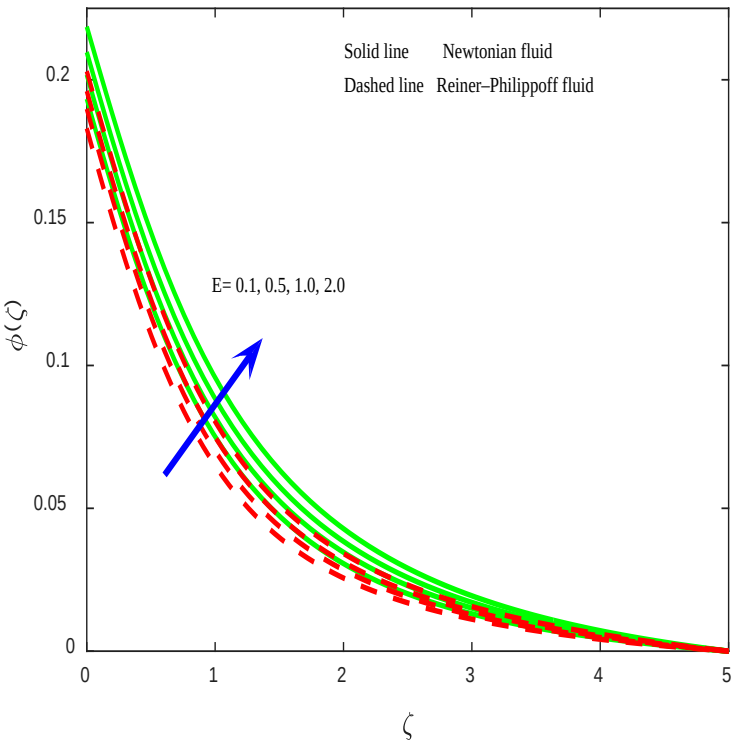

Figure 11. Concentration field for assorted values of E .

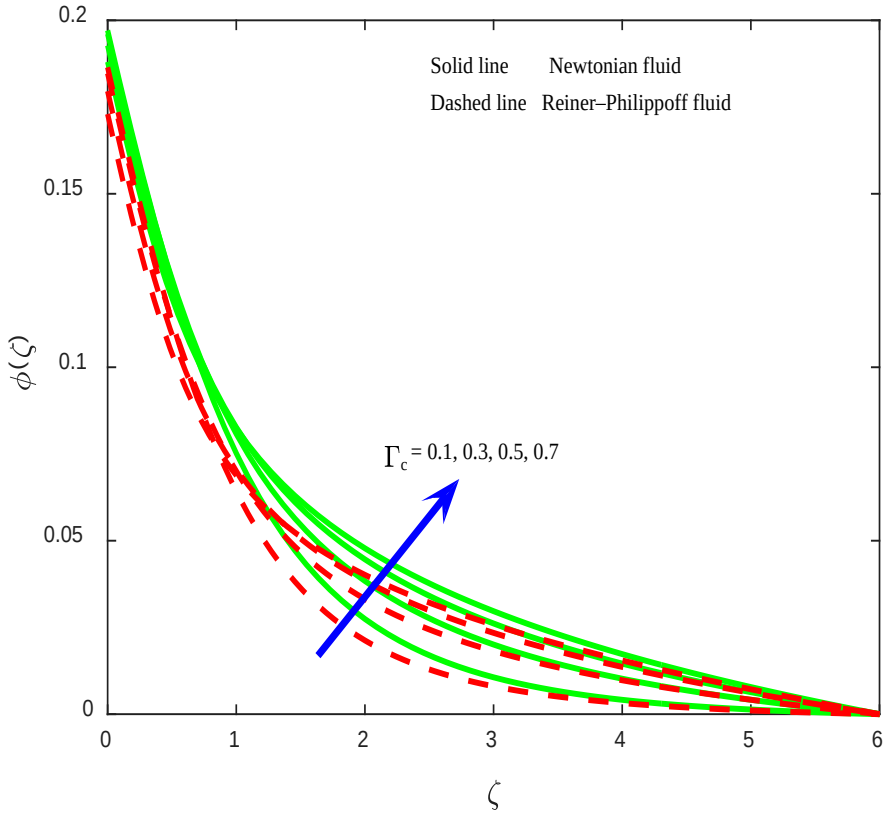

Figure 12. Concentration field for assorted values of Γ_c.

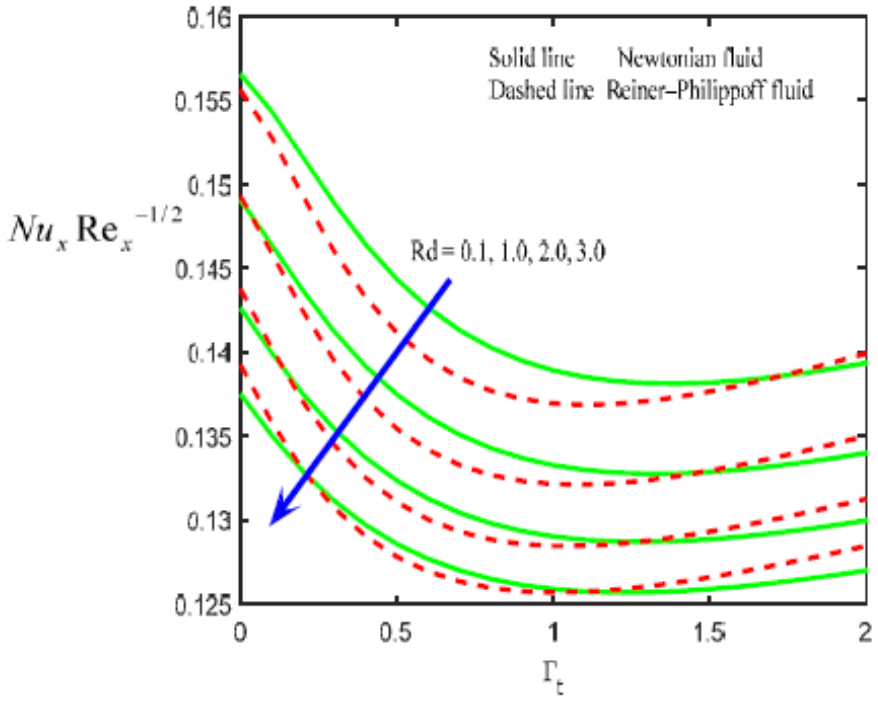

Figure 13. Nusselt number for assorted values of Rd and Γ_t.

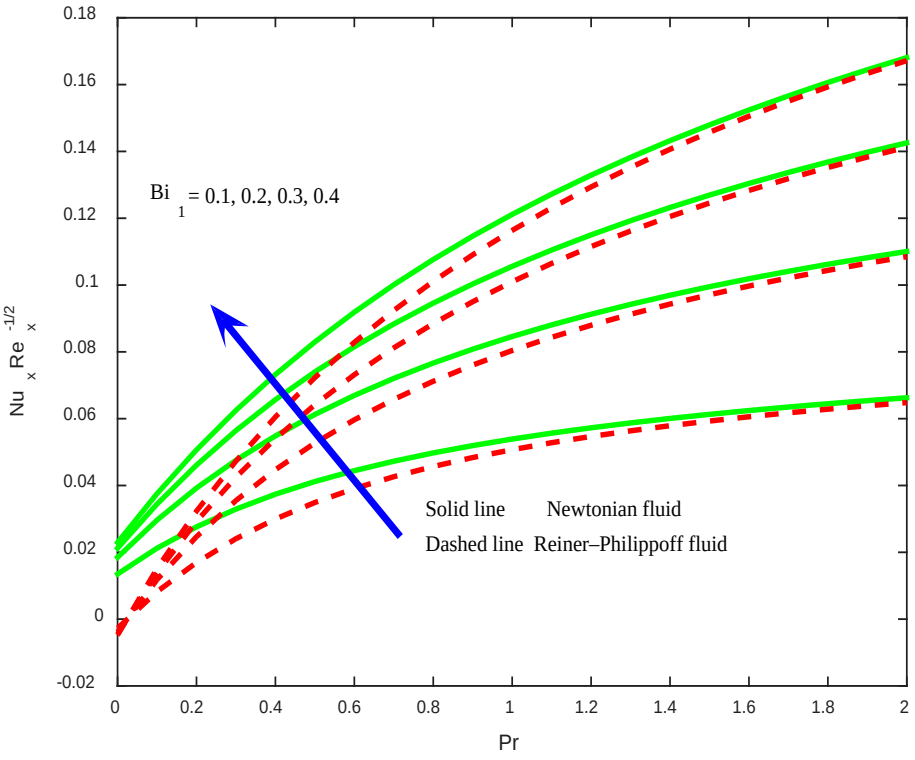

Figure 14. Nusselt number for assorted values of Bi_1 and $\Pr$.

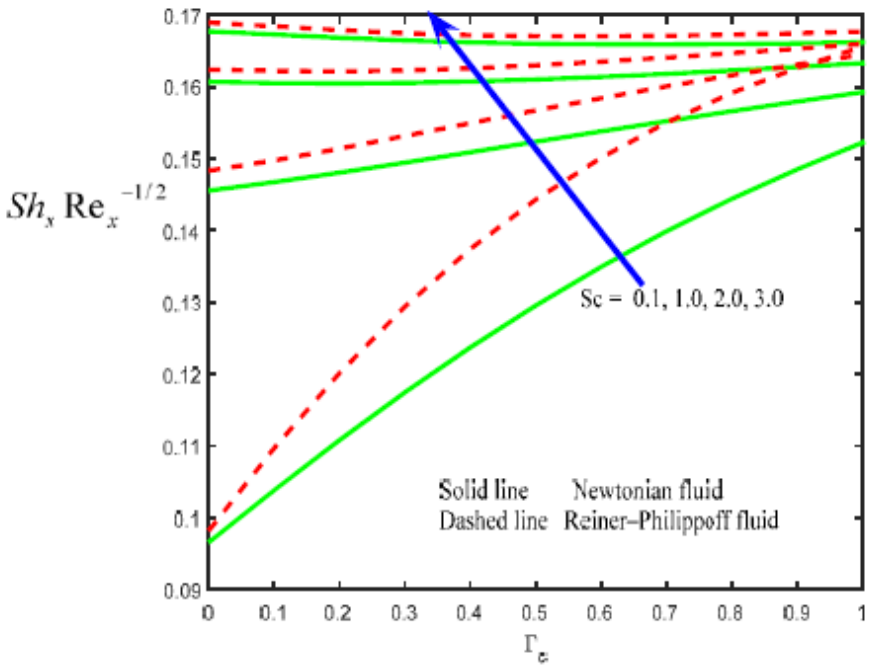

Figure 15. Sherwood number for assorted values of Sc and Γ_t.

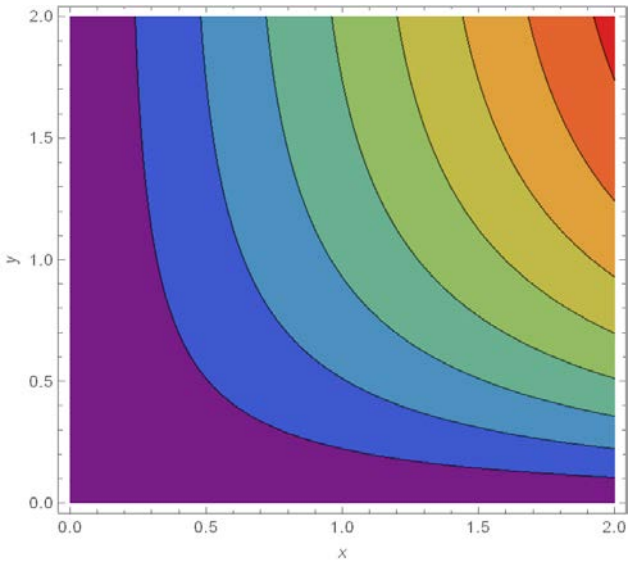

Figure 16. Stream lines for $M = 0.5, \lambda = 1.0$.

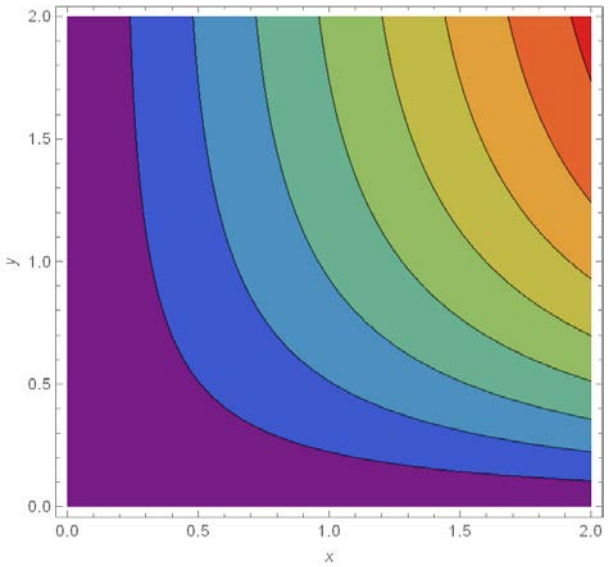

Figure 17. Stream lines for $M = 2.0, \lambda = 1.0$.

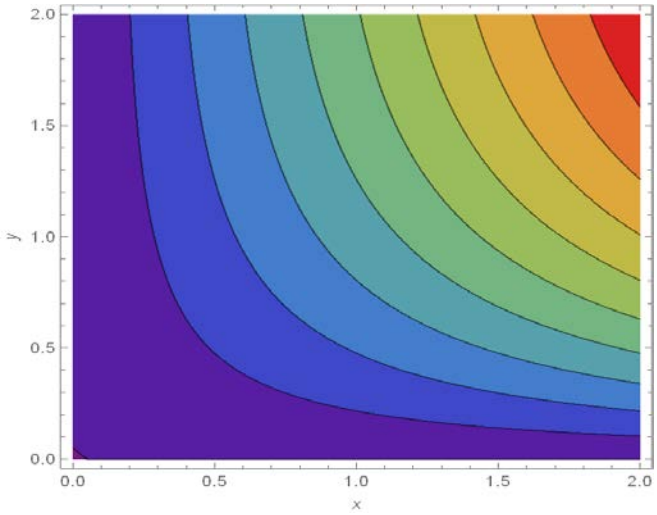

Figure 18. Stream lines for $M = 0.5, \lambda = 2.0$ (Reiner–Philippoff liquid).

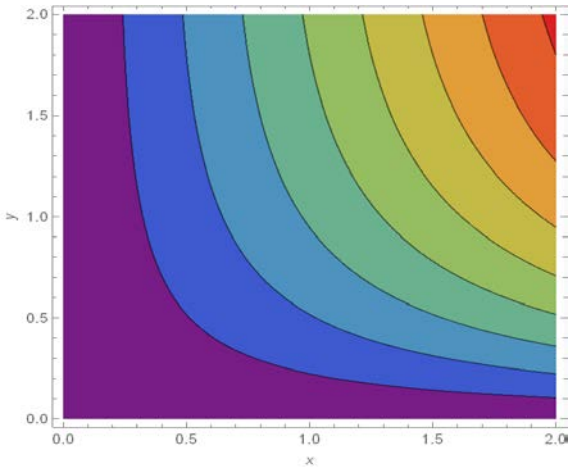

Figure 19. Stream lines for $M = 2.0, \lambda = 2.0$ (Reiner–Philippoff liquid).

5. Conclusions

On a hydromagnetic non-Newtonian fluid with activation energy, a non-linear radiative and Cattaneo–Christov double diffusions (CCDD) flow is investigated. Instead of the classical Fick's and Fourier's laws, the theory of CC double diffusion is used in the modeling. Moreover, convective heat and mass transfer conditions are accounted for in this study. The numerical solution of the converted flow regulating ODE's is given. For both Newtonian and non-Newtonian fluid (Reiner–Philippoff liquid) situations, the generated flow fields of the numerical results are displayed subjected to various influential variables. The key findings are summarized in the following below:

1. The flow field and associated hydrodynamical layer have diminished for Hartmann number Ha.
2. An upsurge in radiation Rd improves the thermal profile.
3. The boundary layer of concentration and thermal distribution exhibit a similar trend for the applied magnetic field.
4. An increase in thermal and solutal relaxation time parameters lead to both the fluid temperature and species concentration being reduced.
5. The impact of thermal and solutal Biot numbers on the energy and concentration have a similar behavior.
6. Species distribution boosts the higher dimensionless activation energy parameter E.
7. The present fluid model is simplified to Newtonian fluid if $\lambda = 1.0$.
8. New numerical schemes based on the homotopy analysis method will be introduced in the future to calculate non-Newtonian nanofluidic problems with several variations.

Author Contributions: Conceptualization, K.M.K., M.E.N. and M.G.R.; methodology, A.M.M. and W.A.; software, M.G.R.; validation, E.A. and K.M.K.; formal analysis, A.M.M. and W.A.; investigation, K.M.K. and E.A.; resources, M.E.N. and E. A.; writing—original draft preparation, A.M.M. and M.G.R.; writing—review and editing, K.M.K., M.E.N. and A.M.M.; visualization, M.E.N. and W.A. All authors have read and agreed to the published version of the manuscript.

Funding: This research received no external funding.

Institutional Review Board Statement: Not applicable.

Informed Consent Statement: Not applicable.

Data Availability Statement: Not applicable.

Conflicts of Interest: The authors declare no conflict of interest.

References

1. Ahmad, A.; Qasim, M.; Ahmed, S. Flow of Reiner–Philippoff fluid over a stretching sheet with variable thickness. *J. Braz. Soc. Mech. Sci. Eng.* **2017**, *39*, 4469–44732017. https://doi.org/10.1007/s40430-017-0840-7.
2. Ullah, A.; Alzahrani, E.O.; Shah, Z.; Ayaz, M.; Islam, S. Nanofluids Thin Film Flow of Reiner-Philippoff Fluid over an Unstable Stretching Surface with Brownian Motion and Thermophoresis Effects. *Coatings* **2018**, *9*, 21. https://doi.org/10.3390/coatings9010021.
3. Kumar, K.G.; Machireddy, G.R.; Sudharani, M.; Shehzad, S.; Chamkha, A.J. Cattaneo–Christov heat diffusion phenomenon in Reiner–Philippoff fluid through a transverse magnetic field. *Phys. A Stat. Mech. Its Appl.* **2020**, *541*, 123330. https://doi.org/10.1016/j.physa.2019.123330.
4. Sajid, T.; Sagheer, M.; Hussain, S. Impact of Temperature-Dependent Heat Source/Sink and Variable Species Diffusivity on Radiative Reiner–Philippoff Fluid. *Math. Probl. Eng.* **2020**, *2020*, 9701860. https://doi.org/10.1155/2020/9701860.
5. Tahir, M.; Ahmad, A. Impact of pseudoplaticity and dilatancy of fluid on peristaltic flow and heat transfer: Reiner-Philippoff fluid model. *Adv. Mech. Eng.* **2020**, *12*, 168781402098118. https://doi.org/10.1177/1687814020981184.
6. Hayat, T.; Qayyum, S.; Shehzad, S.A.; Alsaedi, A. Cattaneo-Christov double-diffusion theory for three-dimensional flow of viscoelastic nanofluid with the effect of heat generation/absorption. *Results Phys.* **2018**, *8*, 489–495. https://doi.org/10.1016/j.rinp.2017.12.060.
7. Iqbal, Z.; Khan, M.; Ahmed, A.; Ahmed, J.; Hafeez, A. Thermal energy transport in Burgers nanofluid flow featuring the Cattaneo–Christov double diffusion theory. *Appl. Nanosci.* **2020**, *10*, 5331–534. https://doi.org/10.1007/s13204-020-01386-y.
8. Khan, M.I.; Hafeez, M.U.; Hayat, T.; Alsaedi, A. Fully developed Darcy-Forchheimer nanomaterial flow with Cattaneo–Christov (CC) double diffusion model. *Mod. Phys. Lett. B* **2020**, *34*, 2050214. https://doi.org/10.1142/s0217984920502140.
9. Ali, B.; Hussain, S.; Nie, Y.; Hussein, A.K.; Habib, D. Finite element investigation of Dufour and Soret impacts on MHD rotating flow of Oldroyd-B nanofluid over a stretching sheet with double diffusion Cattaneo Christov heat flux model. *Powder Technol.* **2021**, *377*, 439–452. https://doi.org/10.1016/j.powtec.2020.09.008.
10. Shehzad, S.A.; Reddy, M.G.; Rauf, A.; Abbas, Z. Bioconvection of Maxwell nanofluid under the influence of double diffusive Cattaneo–Christov theories over isolated rotating disk. *Phys. Scr.* **2020**, *95*, 045207. https://doi.org/10.1088/1402-4896/ab5ca7.
11. Khalil, K.M.; Soleiman, A.; Megahed, A.M.; Abbas, W. Impact of Variable Fluid Properties and Double Diffusive Cattaneo–Christov Model on Dissipative Non-Newtonian Fluid Flow Due to a Stretching Sheet. *Mathematics* **2022**, *10*, 1179. https://doi.org/10.3390/math10071179.
12. Hayat, T.; Muhammad, T.; Shehzad, S.A.; Alsaedi, A. On magnetohydrodynamic flow of nanofluid due to a rotating disk with slip effect: A numerical study. *Comput. Methods Appl. Mech. Eng.* **2017**, *315*, 467–477. https://doi.org/10.1016/j.cma.2016.11.002.
13. Prasannakumara, B.; Machireddy, G.R.; Thammanna, G.; Gireesha, B. MHD Double-diffusive boundary-layer flow of a Maxwell nanofluid over a bidirectional stretching sheet with Soret and Dufour effects in the presence of radiation. *Nonlinear Eng.* **2018**, *7*, 195–205. https://doi.org/10.1515/nleng-2017-0058.
14. Wahid, N.S.; Arifin, N.M.; Turkyilmazoglu, M.; Rahmin, N.A.A.; Hafidzuddin, M.E.H. Effect of magnetohydrodynamic Casson fluid flow and heat transfer past a stretching surface in porous medium with slip condition. *J. Phys. Conf. Ser.* **2019**, *1366*, 012028. https://doi.org/10.1088/1742-6596/1366/1/012028.
15. Qayyum, S.; Khan, M.I.; Chammam, W.; Khan, W.A.; Ali, Z.; Ul-Haq, W. Modeling and theoretical investigation of curved parabolized surface of second-order velocity slip flow: Combined analysis of entropy generation and activation energy. *Mod. Phys. Lett. B* **2020**, *34*, 2050383. https://doi.org/10.1142/s0217984920503832.
16. Radhika, M.; Gowda, R.J.P.; Naveenkumar, R.; Siddabasappa; Prasannakumara, B.C. Heat transfer in dusty fluid with suspended hybrid nanoparticles over a melting surface. *Heat Transf.* **2020**, *50*, 2150–2167. https://doi.org/10.1002/htj.21972.
17. Konduru, S.; Ramanahalli, J.P.G.; Ioannis, E.S.; Rangaswamy, N.K.; Ballajja, C.P. Effect of magnetohydrodynamics on heat transfer behaviour of a non-Newtonian fluid Flow over a stretching sheet under local thermal non-equilibrium condition. *Fluids* **2021**, *6*, 264.
18. Tunde, A.Y.; Fazle, M.; Prasannakumara, B.C.; Ioannis, E.S. Magneto-Bioconvection flow of Williamson nanofluid over an inclined plate with gyrotactic microorganisms and entropy generation. *Fluids* **2021**, *6*, 109.
19. Hasan, S.; Xinhua, W.; Ioannis, S.; Kaleem, I.; Muhammad, B.H.; Marek, K. Study of Non-Newtonian biomagnetic blood flow in a stenosed bifurcated artery having elastic walls. *Sci. Rep.* **2021**, *11*, 23835.
20. Ramanahalli, J.P.G.; Rangaswamy, N.K.; Anigere, M.J.; Ballajja, C.P.; Ioannis, E.S. Impact of binary chemical reaction and activation energy on heat and mass transfer of marangoni driven boundary layer flow of a non-Newtonian nanofluid. *Processes* **2021**, *9*, 702.
21. Megahed, A.M.; Reddy, M.G.; Abbas, W. Modeling of MHD fluid flow over an unsteady stretching sheet with thermal radiation, variable fluid properties and heat flux. *Math. Comput. Simul.* **2021**, *185*, 583–593. https://doi.org/10.1016/j.matcom.2021.01.011.
22. Abbas, W.; Megahed, A.M. Numerical solution for chemical reaction and viscous dissipation phenomena on non-Newtonian MHD fluid flow and heat mass transfer due to a nonuniform stretching sheet with thermal radiation. *Int. J. Mod. Phys. C* **2021**, *32*, 2150124. https://doi.org/10.1142/s0129183121501242.
23. Kumar, K.G.; Gireesha, B.J.; Prasannakumara, B.; Ramesh, G.; Makinde, O.D. Phenomenon of Radiation and Viscous Dissipation on Casson Nanoliquid Flow Past a Moving Melting Surface. *Diffus. Found.* **2017**, *11*, 33–42. https://doi.org/10.4028/www.scientific.net/df.11.33.

24. Qayyum, S.; Khan, M.I.; Hayat, T.; Alsaedi, A. A framework for nonlinear thermal radiation and homogeneous-heterogeneous reactions flow based on silver-water and copper-water nanoparticles: A numerical model for probable error. *Results Phys.* **2017**, *7*, 1907–1914. https://doi.org/10.1016/j.rinp.2017.05.020.
25. Prasannakumara, B.; Gireesha, B.; Krishnamurthy, M.; Kumar, K.G. MHD flow and nonlinear radiative heat transfer of Sisko nanofluid over a nonlinear stretching sheet. *Inform. Med. Unlocked* **2017**, *9*, 123–132. https://doi.org/10.1016/j.imu.2017.07.006.
26. Hayat, T.; Kanwal, M.; Qayyum, S.; Alsaedi, A. Entropy generation optimization of MHD Jeffrey nanofluid past a stretchable sheet with activation energy and non-linear thermal radiation. *Phys. A Stat. Mech. Its Appl.* **2020**, *544*, 123437. https://doi.org/10.1016/j.physa.2019.123437.
27. Khan, M.I.; Qayyum, S.; Waqas, M.; Hayat, T.; Alsaedi, A. Framing the novel aspects of irreversibilty in MHD flow of Williamson nanomaterial with thermal radiation near stagnation point. *J. Therm. Anal.* **2019**, *139*, 1291–1299. https://doi.org/10.1007/s10973-019-08524-x.
28. Khan, M.I.; Qayyum, S.; Hayat, T.; Waqas, M.; Alsaedi, A. Entropy generation minimization and binary chemical reaction with Arrhenius activation energy in MHD radiative flow of nanomaterial. *J. Mol. Liq.* **2018**, *259*, 274–283. https://doi.org/10.1016/j.molliq.2018.03.049.
29. Qayyum, S.; Hayat, T.; Kanwal, M.; Alsaedi, A.; Khan, M.I. Transportation of entropy optimization in radiated chemically dissipative flow of Prandtl–Eyring nanofluid with activation energy. *Comput. Methods Programs Biomed.* **2020**, *184*, 105130. https://doi.org/10.1016/j.cmpb.2019.105130.
30. Kotresh, M.J.; Ramesh, G.K.; Shashikala, V.K.R.; Prasannakumara, B.C. Assessment of Arrhenius activation energy in stretched flow of nanofluid over a rotating disc. *Heat Transf.* **2020**, *50*, 2807–2828. https://doi.org/10.1002/htj.22006.
31. Khan, M.I.; Alzahrani, F. Activation energy and binary chemical reaction effect in nonlinear thermal radiative stagnation point flow of Walter-B nanofluid: Numerical computations. *Int. J. Mod. Phys. B* **2020**, *34*, 2050132. https://doi.org/10.1142/s0217979220501325.
32. Jayadevamurthy, P.G.R.; Rangaswamy, N.K.; Prasannakumara, B.C.; Nisar, K.S. Emphasis on unsteady dynamics of bioconvective hybrid nanofluid flow over an upward–downward moving rotating disk. *Numer. Methods Part. Differ. Equ.* **2020**, 22680. https://doi.org/10.1002/num.22680.
33. Shehzad, S.; Hayat, T.; Alsaedi, A. Influence of convective heat and mass conditions in MHD flow of nanofluid. *Bull. Pol. Acad. Sci. Tech. Sci.* **2015**, *63*, 465–474. https://doi.org/10.1515/bpasts-2015-0053.
34. Prasannakumara, B.; Gireesha, B.; Krishnamurthy, M.; Gorla, R.S.R. Slip flow and nonlinear radiative heat transfer of suspended nanoparticles due to a rotating disk in the presence of convective boundary condition. *Int. J. Nanopart.* **2017**, *9*, 180. https://doi.org/10.1504/ijnp.2017.089212.
35. Hayat, T.; Saif, R.S.; Ellahi, R.; Muhammad, T.; Ahmad, B. Numerical study of boundary-layer flow due to a nonlinear curved stretching sheet with convective heat and mass conditions. *Results Phys.* **2017**, *7*, 2601–2606. https://doi.org/10.1016/j.rinp.2017.07.023.
36. Gireesha, B.; Kumar, K.G.; Ramesh, G.; Prasannakumara, B. Nonlinear convective heat and mass transfer of Oldroyd-B nanofluid over a stretching sheet in the presence of uniform heat source/sink. *Results Phys.* **2018**, *9*, 1555–1563. https://doi.org/10.1016/j.rinp.2018.04.006.
37. Muhammad, K.; Hayat, T.; Alsaedi, A. Squeezed flow of Jeffrey nanomaterial with convective heat and mass conditions. *Phys. Scr.* **2019**, *94*, 105703. https://doi.org/10.1088/1402-4896/ab234f.